RESEARCH ARTICLE | NOVEMBER 03 2025

Saturation and decay of an induced scattering instability driven by static field asymmetries in a non-neutral plasma

D. L. Eggleston

Phys. Plasmas 32, 112104 (2025)
https://doi.org/10.1063/5.0292762
CHORUS

Physics of Plasmas ARTICLE pubs.aip.org/aip/pop

Saturation and decay of an induced scattering instability driven by static field asymmetries in a non-neutral plasma

Cite as: Phys. Plasmas **32**, 112104 (2025); doi: 10.1063/5.0292762
Submitted: 23 July 2025 · Accepted: 17 October 2025 ·
Published Online: 3 November 2025

D. L. Eggleston[a)]

AFFILIATIONS

Physics Department, Occidental College, Los Angeles, California 90041, USA

[a)]Author to whom correspondence should be addressed: eggleston@oxy.edu

ABSTRACT

Experimental data on the saturation and decay of a previously described induced scattering instability are presented. The instability is driven by static background field asymmetries and initially produces a single growing mode (ω_1, k_1). As the instability develops, several harmonically related ($\omega_n = n\omega_1$, $k_n = nk_1$) eigenmodes of the plasma column grow up, resulting in a spatially localized moving potential perturbation with $\delta\phi/T \approx 20\%$. After a period of rapid growth, the mode amplitudes saturate and vary slowly for roughly $10^5\ \omega_1^{-1}$. This quasi-equilibrium ends with an unusual change in the eigenmode phases, wherein $\delta\phi$ changes from positive to negative. Plasma heating during this period increases the damping of all modes and rapidly quenches the instability. This instability is of particular interest because the coupling with the field asymmetry produces an enhanced level of radial transport.

I. INTRODUCTION

Some time ago, Eggleston and Malmberg[1] presented experiments showing an example of an induced scattering instability driven by static field asymmetries in a pure electron plasma of column length L. The unstable mode driven was a standing electron plasma wave with azimuthal and axial wave numbers $l = 0$ and $k = \pi/L$, sometimes called a Trivelpiece-Gould mode. The size of the asymmetry and the damping of the mode were varied experimentally, and the identification of the instability as an induced scattering type was solidified by agreement with supporting theoretical work.[2,3] Contemporaneous data on the long-term evolution (saturation and decay) of this instability when driven by static background asymmetries were presented at a conference,[4] but never published. This paper presents these data.

II. EXPERIMENTAL DEVICE

The experiments were performed on the Malmberg–Penning trap (denoted V') shown schematically in Fig. 1. The device consists of a long cylinder (wall radius $R = 3.05$ cm) divided axially into cylinders of various lengths (here called "rings") and placed into a uniform axial magnetic field $B \leq 675$ G. Two of the rings, labeled S1 and S2, are divided azimuthally into four equal sectors, denoted A to D. The operation is standard for a Malmberg-Penning trap.[5] Typically, two of the rings (here G1 and G3) are held at a large negative potential. To start a cycle, G1 is grounded, allowing electrons from a negatively biased source to fill the device. Ring G1 is then returned to its negative potential, thus trapping the electrons between G1 and G3. At a selected time later, G3 is grounded, allowing the electrons to leave the trap, and the line-integrated charge is measured by positively biased collectors. When the radially movable collector is used, a radial density profile can be constructed from many shots due to the excellent shot-to-shot reproducibility of these traps. An example of the roughly bell shaped profile is given in Fig. 11 of Ref. 5. Axial temperature is measured using the technique detailed in Ref. 6. Typical parameters for these experiments are electron density $n_e \approx 7 \times 10^6\ \mathrm{cm}^{-3}$, axial temperature $T_e \approx 1$ eV, axial magnetic field $B_z = 350$ G, vacuum pressure 10^{-10} Torr, and plasma lifetime approximately 500 ms. The inner distance between the confinement rings G1 and G3 is 113.7 cm, but the plasma is slightly compressed by the confinement potentials. We estimate the column length L to be 108 cm.

III. EXPERIMENTAL RESULTS

As detailed in Ref. 1, it is found that under a broad range of conditions, a plasma mode spontaneously grows after the electrons are trapped, driven by static background field asymmetries. The evolution

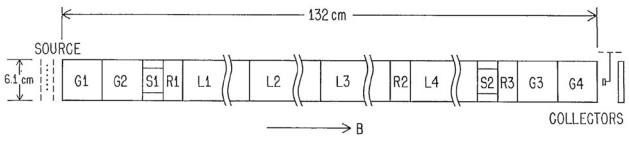

FIG. 1. Schematic of the experimental device. Electrically isolated cylinders of various lengths are arranged on a common axis and immersed in a uniform axial magnetic field. Two of the cylinders (marked S1 and S2) are divided azimuthally into four equal sectors allowing one to detect or apply potentials with azimuthal variation.

of the instability can be viewed in two complementary ways. Both ways use the variation of charge on one of the shorter rings or sectors (e.g., R1 or S1D) encircling the trapped electrons to measure the unstable mode amplitude. The ring is connected to an amplifier (gain 20–40 dB) with an input impedance of 50 or 1000 Ω. The first method connects the output of this amplifier to a spectrum analyzer set to zero-scan mode. In this mode, the spectrum analyzer acts as a tuned filter, giving an output proportional to the logarithm of the signal amplitude at a selected frequency. The bandwidth of the analyzer is set to 100 or 300 kHz (to ensure good time response) and the frequency adjusted to find one of the constituent frequencies of the signal.

An example of a signal obtained using this method is shown in Fig. 2. In this case, the spectrum analyzer is set to a frequency of 810 kHz. The trace marked *a* shows the unstable mode growing immediately upon the creation of the electron plasma at t = 0. For curve *b*, we suppress the mode by increasing its damping until the time marked by the lower arrow, at which time the damping is switched off and the mode grows. The damping is increased by adding a resistor to ground on one of the larger rings (e.g., L2). Since the unstable mode is a positive energy wave, Ohmic loses to this resistor damp the wave. This damping can be added or removed by switching the resistor's connection to the ring with a relay. For curve *c*, the mode grows as in case *a* until the time marked by the upper arrow. At this point, the damping is increased, and the mode decays.

The second, and more direct, way to view the unstable mode is to display the wall probe signal on an oscilloscope. This is shown in Fig. 3. At the center of the figure is the output of the spectrum analyzer (proportional to the logarithm of the signal amplitude at $f = 810$ kHz) vs time, showing the full evolution of the unstable mode. At selected times, we show the oscilloscope traces of a few cycles of the unstable mode. For each oscilloscope photo, the upper trace shows the raw signal coming out of the amplifier. For the lower trace, we route the raw signal to an op-amp integrator circuit ($R = 10\,k\Omega$, $C = 1\,\mu$F) and display the output. This latter trace is relevant because the raw signal is proportional to the time derivative of the mode amplitude, so its integral shows the mode amplitude itself.[15] The displayed sequence of oscilloscope traces shows how the instability starts as a sinusoidal signal but then sharpens to become a non-sinusoidal localized waveform.[16] By simultaneously observing the signal on more than one ring, we have verified that this localized waveform propagates back and forth axially along the plasma column with a speed of approximately 1.7×10^8 cm/s. At later times, this localized waveform inverts and then decays.

Numerical solutions of the linearized drift-kinetic and Poisson's equations (see Appendix) give the radial dependence of the eigenmode potential for each (ω_n, k_n). Summing these and accounting for the small axial potential variations across the ring electrode allows us to determine the localized waveform amplitude $\delta\phi$ from the wall probe

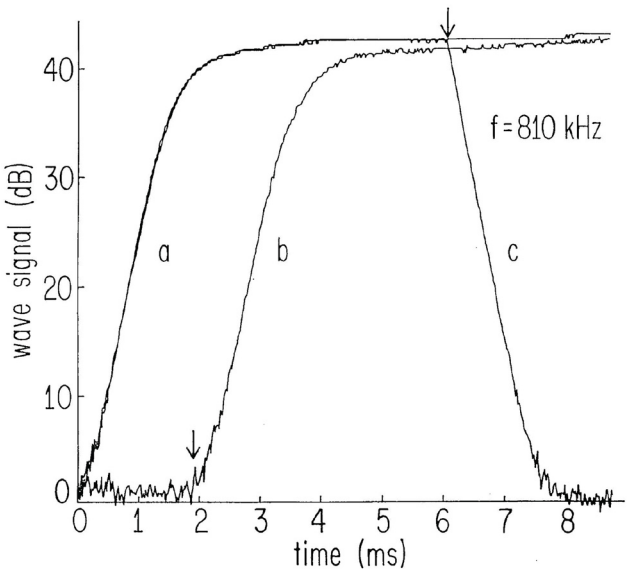

FIG. 2. Time evolution of the unstable mode driven by background field asymmetries. Curve a: Mode grows immediately upon creation of plasma. Curve b: Mode remains stable until damping is decreased, and threshold is exceeded. Curve c: Unstable mode is stabilized by increasing the mode damping. Each curve is from a single plasma shot. Reproduced with permission from Eggleston and Malmberg, Phys. Rev. Lett. **59**, 1675 (1987). Copyright 1987 American Physical Society.

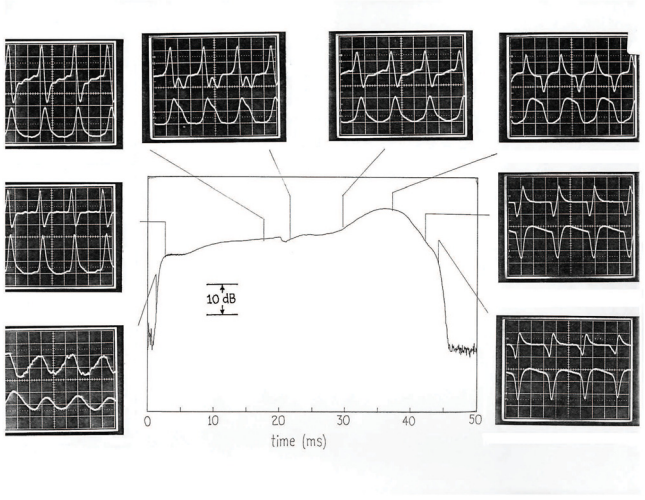

FIG. 3. The logarithm of the instability amplitude vs time (central plot) together with selected oscilloscope traces at the times indicated showing how the instability becomes a localized waveform and then inverts. For each oscilloscope photo, the upper trace shows the raw signal, and the lower trace shows the output of an op-amp integrator circuit. The timescale for all photos is 0.5 μs/div. Note the voltage scale changes for the various photos. Starting at the lower left photo and proceeding clockwise, the scale for the upper (lower) trace is 2 mV/div (50 mV/div), 20 mV/div (0.2 V/div), 20 mV/div (0.5 V/div), 20 mV/div (0.5 V/div), 50 mV/div (1.0 V/div), 0.1 V/div (2.0 V/div), 0.1 V/div (1.0 V/div), and 20 mV/div (0.2 V/div). Times for the photos (in ms) are 1.2, 2.5, 17.5, 21.5, 29.5, 37.0, 42.0, and 44.0.

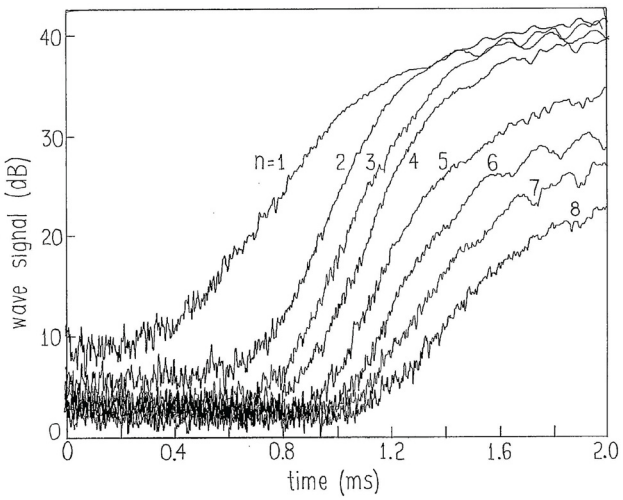

FIG. 4. The time evolution of the first eight harmonics. The wave signal is the output of a spectrum analyzer tuned to the various harmonic frequencies.

signals. Using this method, we estimate $\delta\phi/T \approx 20\%$ when the instability is saturated. We note, however, that this calculation assumes the localized waveform is simply a superposition of linear modes rather than a nonlinear entity, which may have a different radial dependence.

The sharpening of the oscilloscope traces implies the presence of higher frequency and wavenumber harmonics in the instability, and this can be seen clearly in Fig. 4. Here, we display the output of the spectrum analyzer vs time. The various traces show the output with the spectrum analyzer set to one of the first eight harmonic frequencies. Initially, only the first harmonic is above the noise level, but as the first harmonic grows, we begin to see a second harmonic rise above the noise level, and so on with the higher harmonics. The sharpening of the oscilloscope traces demonstrates that these harmonics are in phase.

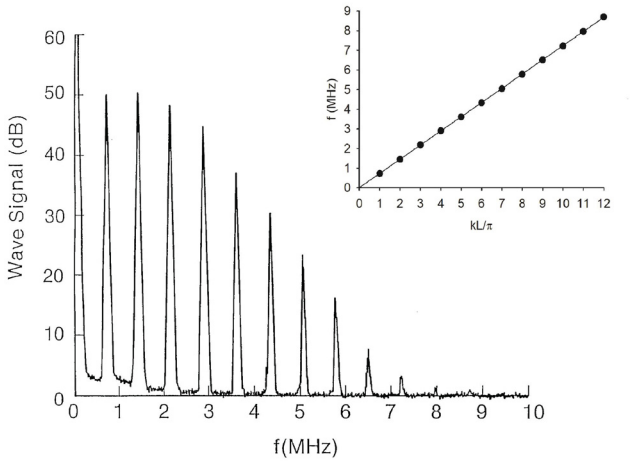

FIG. 5. Spectrum of the fully developed instability, showing that it consists of harmonics of the $n = 1$ mode. Here, the spectrum analyzer bandwidth was 30 kHz. The inset shows the resulting dispersion relation showing the linear relation typical of $l = 0$ plasma modes in a bounded plasma.

An alternate way of representing this development is to display the spectrum of the unstable mode after it is fully developed (t = 14 ms). This is shown in Fig. 5. The main plot is generated by slowly (∼100 s) sweeping the spectrum analyzer frequency, sampling the output at the selected time (14 ms) and displaying the result on a chart recorder. The plot is, thus, constructed from many experimental cycles and made possible by the excellent shot-to-shot reproducibility.

We assume that the higher harmonic frequencies ω_n are occurring at higher wavenumbers k_n. Although the apparatus does not allow for a determination of k from a continuous measurement of the mode potential vs axial position, we can simultaneously view wall probe signals at various axial positions, noting the relative phases and amplitudes. Such data are in agreement with our assumption. We, thus, show in the inset of Fig. 5 the resulting experimental dispersion

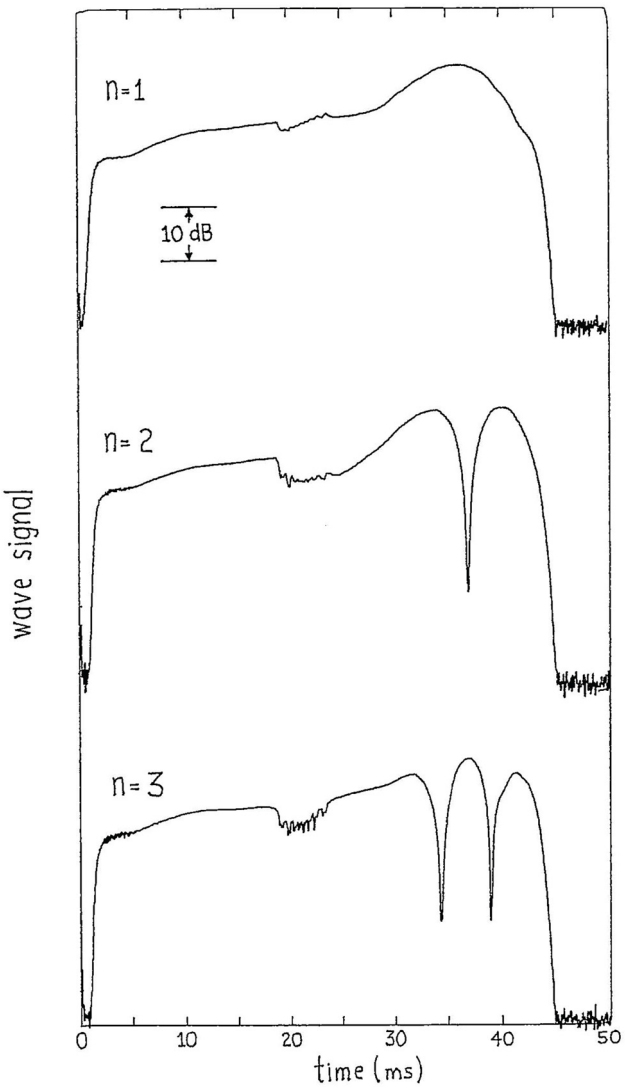

FIG. 6. Output of spectrum analyzer tuned to harmonics 1–3 vs time showing deep amplitude dips.

relation. Such modes have been identified as $l = 0$, $k = n\pi/L$ plasma waves in launch and detect experiments on long, stable plasmas in the same experimental device observing modes up to $n = 29$ with theory matching experiment to within experimental error. Note that for those experiments, the dispersion relation is visually linear up to $n = 10$ (see Fig. 3 in Malmberg *et al.*[5]).

While Fig. 4 shows the early growth of the first eight harmonics, it is also interesting to view the long-term evolution of some of these frequencies. This is shown in Figs. 6 and 7. Of particular interest are the deep (~ 30 dB) amplitude dips seen at later times for $n = 2$–6 but not $n = 1$. These appear to be associated with the inversion of the localized waveform. Other notable features are the long period between dips and the simple relation between the number of dips D and the harmonic number (i.e., $D = n - 1$).

The ability to quench the instability by adding damping allows us to see the effect of the instability on other plasma parameters. This is shown in Figs. 8 and 9 for total confined particles per unit column length N_{tot} and axial temperature T, respectively. Measurements of the radial density profile (not shown) confirm that the loss of confined charge is due to outward radial transport. At first glance, this is perplexing since the unstable modes have $l = 0$, thus no azimuthal variation in potential and no radial $E \times B$ drift. In fact, this increased radial transport is further evidence that the instability is driven by field asymmetries, and the transport is produced by the coupling between the unstable mode and the field asymmetry. The radial particle transport is accompanied by an increase in the axial temperature, as shown in Fig. 9.

We also note that spontaneous growth of the instability was not observed for shorter plasma columns ($L < 85$ cm), probably due to the decreased amplitude of the driving asymmetries as inferred from transport experiments.[7,8] This would also explain why this instability has not been observed, to our knowledge, in other, shorter Malmberg-

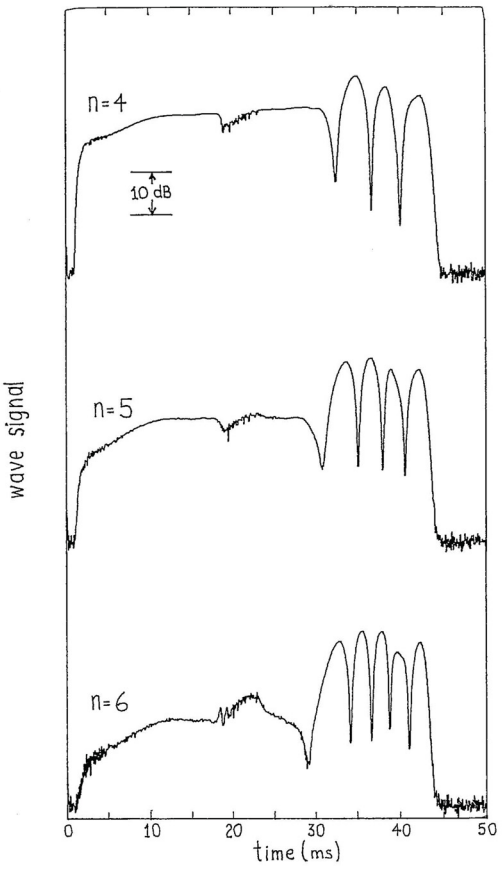

FIG. 7. Output of spectrum analyzer tuned to harmonics 4–6 vs time showing deep amplitude dips.

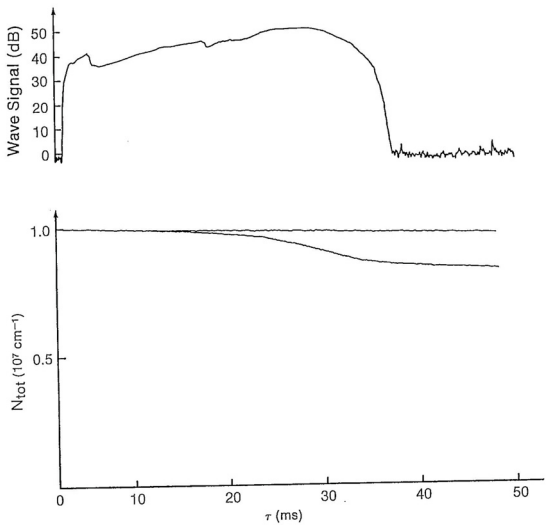

FIG. 8. Upper graph shows the instability amplitude vs time. Lower graph shows two plots of the total number of electrons confined in the device vs time. The upper plot shows data when the instability is suppressed with a resistor from a ring to ground, while the lower plot shows increased loss when the instability is allowed to grow.

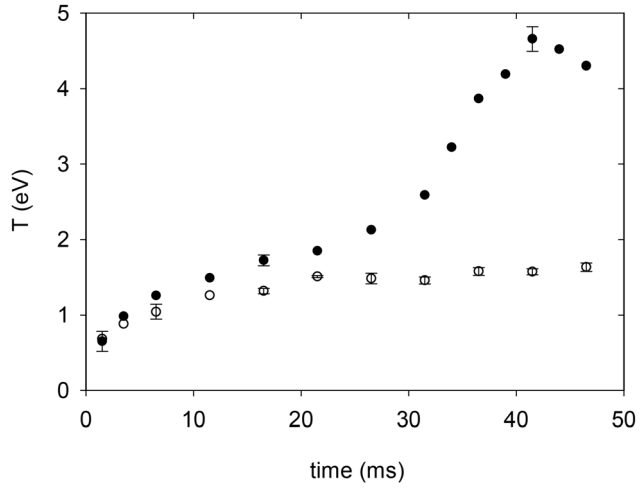

FIG. 9. Axial electron temperature vs time. The lower curve (open symbols) shows the data when the instability is suppressed, while the upper curve (solid symbols) shows the data when the instability is allowed to develop. Representative error bars are shown on some of the data points.

Penning traps. However, even for these shorter columns we were able to induce the instability by applying a short signal burst to one of the rings at the $l = 0$, $n = 1$ mode frequency. Presumably, driving the mode produces sufficient decrease in the damping (through modification of the velocity distribution) to satisfy the instability condition.[17]

As noted above, our detection of the instability involves connecting a signal amplifier to one of the shorter rings. We have checked that the amplifier input impedance does not affect the instability by switching in and out the amplifier connection to the ring at various times. The observed evolution of the instability is unchanged. Presumably, this is because the shorter rings have less image charge and thus produce less current into the amplifier and less ohmic loss.

Observing the instability using a narrower bandwidth (10 kHz) on the spectrum analyzer shows that the frequency of the primary mode changes by approximately 100 kHz over the evolution of the instability, decreasing in time until about 40 ms and then increasing. This is not seen in Figs. 2–8 since the frequency variation is within the 100–300 kHz bandwidth used to acquire those data. While we do not understand this frequency variation, it could be due to the fact that the mode frequency depends on the density and axial temperature profiles, and these are changing over time.

We also note the peculiar dip occurring at approximately 20 ms in the plots of Figs. 6 and 7. As shown in the photos of Fig. 3, these cause a momentary change in the shape of the localized waveform. The cause of this phenomena is not understood, but we note that it occurs at roughly the same time that changes in N_{tot} and T begin.

IV. DISCUSSION

The experimental conditions for our results include a number of elements that make theoretical modeling difficult: a continuous drive from the background asymmetry through the induced scattering process, mode damping associated with a warm plasma, radially dependent density and temperature profiles, and concurrent transport in both velocity space and configuration space. Nevertheless, we offer a simple model that explains some of the main features of the long-term evolution while acknowledging that other explanations may be possible: (1) As the first harmonic ($n = kL/\pi = 1$) of the unstable mode grows and becomes nonlinear, the second harmonic ($n = 2$) is driven and grows. The nonlinear combination of the $n = 1$ and $n = 2$ modes then drives the $n = 3$ mode and so on. (2) The combination of these harmonics produces a localized waveform, which moves back and forth between the axial confinement cylinders. (3) The cause and features of the late-time amplitude dips are not well understood. The depth of the dips and the long period between dips suggest a slow "beating" phenomena.[18] The data show that initially, the dispersion relation for the plasma waves is linear in k, which produces the harmonic relations facilitating the process of part (1). To explain the late-time amplitude dips, we posit a small, k-dependent deviation from linearity due to changes in the plasma conditions (density and temperature profiles) at late times. Such a deviation from linearity is plausible since we know that this happens at higher k values in drive and detect experiments.[5] Because of this deviation, the frequency of the $n = 2$ mode is now not quite twice the $n = 1$ frequency. A resonant system driven slightly off resonance exhibits slow sinusoidal variations in the amplitude of the response at a frequency equal to the difference between the drive frequency and the resonant frequency (i.e., "beats"). The deviation from linearity, thus, produces a beat in the $n = 2$ amplitude, as seen in the data. A similar process affects the higher k amplitudes, but with a higher beat frequency, again in accord with the data. This model also explains why there is no dip in the $n = 1$ amplitude. (4) This beating alters the particular phase relation between the harmonics that produced the original localized waveform, producing an inverted localized waveform. (5) The linkage of these modes with the driving field asymmetry produces increased radial transport and a concurrent increase in the axial temperature T, which increases the mode damping enough so that the instability condition is no longer satisfied, and all modes decay to zero.

Finally, we note that, because the physical basis for these processes is fairly general, these results may be relevant to other rotating plasmas subject to field asymmetries (e.g., stellarators, tandem mirrors, and tokamaks). This would be of especial interest due to the enhanced level of radial transport associated with the presence of the instability.

V. CONCLUSION

We have presented data on the saturation and decay of an induced scattering instability in a non-neutral plasma. As the instability grows, harmonically related eigenmodes are driven and contribute to the formation of a localized waveform. This state persists for roughly $10^5\ \omega_1^{-1}$, where ω_1 is the angular frequency of the fundamental mode. At later times, there occurs a peculiar series of dips in the amplitudes of the harmonics along with concurrent radial transport and plasma heating. The instability then decays to zero. A simple qualitative model explains these features.

ACKNOWLEDGMENTS

This paper is based upon data acquired during support by the U.S. Department of Energy under Grant Nos. DE-FG03-85ER53199 and NSF PHY83-06077. The author acknowledges useful conversations with Tom O'Neil and John David Crawford. The paper is dedicated to the memory of Professor John Malmberg.

AUTHOR DECLARATIONS

Conflict of Interest

The author has no conflicts to disclose.

Author Contributions

D. L. Eggleston: Conceptualization (lead); Data curation (lead); Formal analysis (lead); Investigation (lead); Methodology (lead); Software (lead); Visualization (lead); Writing – original draft (lead); Writing – review & editing (lead).

DATA AVAILABILITY

The data that support the findings of this study are available from the corresponding author upon reasonable request.

APPENDIX: NUMERICAL SOLUTION FOR THE MODE POTENTIAL

It has previously been shown[9] that low frequency modes with axial and azimuthal wavenumbers k and l in a non-neutral plasma column are governed by

$$\left(\frac{1}{r}\frac{d}{dr}r\frac{d}{dr}-\frac{l^2}{r^2}-k^2\right)\phi_1 = \frac{e^2}{m\epsilon_0}\left[\int_{-\infty}^{\infty}dv\frac{k\partial f_0/\partial v-(l/r\omega_c)(\partial f_0/\partial r)}{w-l\omega_R(r)-kv}\right]\phi_1, \tag{A1}$$

where $\phi_1(r)$ is the mode potential, ω is the (generally complex) mode angular frequency, v is the axial velocity, ω_R is the $E\times B$ rotation frequency, and ω_c is the cyclotron frequency. Assume a distribution function given by

$$f_0=\frac{n_0(r)}{\sqrt{\pi}a(r)}\exp\left(-\frac{v^2}{a^2(r)}\right), \tag{A2}$$

where $a(r)=\sqrt{2}\bar{v}(r)=\sqrt{2T(r)/m}$. Then, using the plasma dispersion function $Z(s)$,[10] Eq. (A1) may be written as

$$\left(\frac{1}{r}\frac{d}{dr}r\frac{d}{dr}-\frac{l^2}{r^2}-k^2\right)\phi_1 = \left[2\left(\frac{\omega_p}{a}\right)^2[1+sZ(s)]\left(1+\frac{ls}{rk\omega_c}\frac{da}{dr}\right)+\frac{l}{rk\omega_c}Z(s)\frac{d}{dr}\left(\frac{\omega_p^2}{a}\right)\right]\phi_1 \tag{A3}$$

or

$$\left(\frac{1}{r}\frac{d}{dr}r\frac{d}{dr}-\frac{l^2}{r^2}-k^2\right)\phi_1 = \left[\frac{l}{rk\omega_c}Z(s)\frac{d}{dr}\left(\frac{\omega_p^2}{a}\right)-\left(\frac{\omega_p}{a}\right)^2Z'(s)\left(1+\frac{ls}{rk\omega_c}\frac{da}{dr}\right)\right]\phi_1, \tag{A4}$$

where $s=(\omega-l\omega_R)/ka$ and w_p is the plasma frequency, and we have used $1+sZ(s)=-Z'(s)/2$. This equation can be solved numerically for given k and any given density and temperature profiles by dividing the range of r values into many steps of value Δr and expressing the derivatives on the left hand side as finite differences [see Eq. (36) in Ref. 11]. The procedure is then as follows. We make an initial guess ω_a for the complex frequency ω. For the $l=0$ mode, we take $\phi_1(r=0)$ to be some constant and $\phi_1(r=\Delta r)$ to be a slightly smaller constant. These assumptions are enough to start the finite difference solutions, and the results can be stepped all the way to the wall radius R. This is referred to as the "shooting" method. The resulting complex potential at the wall (call it ϕ_a) will typically not match the required boundary condition $\phi_1(R)=0$. So we make another, slightly different guess ω_b for the complex frequency and follow the same procedure to obtain a second wall potential ϕ_b. We then assume these wall potentials and ω are linearly related: $\omega_a=\alpha\phi_a+\beta$ and $\omega_b=\alpha\phi_b+\beta$. Eliminating α, we obtain $\beta=(\omega_a\phi_b-\omega_b\phi_a)/(\phi_b-\phi_a)$. Since we want $\phi_1(R)=0$, our next guess for ω is $\omega_c=\alpha\phi_c+\beta=\beta$. We shoot again and iterate the procedure until the potential at the wall is sufficiently close to the desired value of zero. The solution gives both $\phi_1(r)$ and the complex frequency ω.

REFERENCES

[1]D. L. Eggleston and J. H. Malmberg, Phys. Rev. Lett. **59**, 1675 (1987).
[2]J. D. Crawford, T. M. O'Neil, and J. H. Malmberg, Phys. Rev. Lett. **54**, 697 (1985).
[3]J. D. Crawford and T. M. O'Neil, Phys. Fluids **30**, 2076 (1987).
[4]D. L. Eggleston and J. H. Malmberg, Bull. Am. Phys. Soc. **32**, 1755 (1987).
[5]J. H. Malmberg, C. F. Driscoll, B. Beck, D. L. Eggleston, J. Fajans, K. Fine, X.-P. Huang, and A. W. Hyatt, "Experiments with pure electron plasmas," in *Non-Neutral Plasma Physics*, edited by C. W. Roberson and C. F. Driscoll (American Institute of Physics, New York, 1988).
[6]D. L. Eggleston, C. F. Driscoll, B. R. Beck, A. W. Hyatt, and J. H. Malmberg, Phys. Fluids B **4**, 3432 (1992).
[7]C. F. Driscoll and J. H. Malmberg, Phys. Rev. Lett. **50**, 167 (1983).
[8]C. F. Driscoll, K. S. Fine, and J. H. Malmberg, Phys. Fluids **29**, 2015 (1986).
[9]J. S. DeGrassie and J. H. Malmberg, Phys. Fluids **23**, 63 (1980).
[10]B. F. Fried and S. Conte, *The Plasma Dispersion Function* (Academic, New York, 1961).
[11]D. L. Eggleston and T. M. O'Neil, Phys. Plasmas **6**, 2699 (1999).
[12]W. Bertsche, J. Fajans, and L. Friedland, Phys. Rev. Lett. **91**, 265003 (2003).
[13]M. Affolter, F. Anderegg, D. H. E. Dubin, F. Valentini, and C. F. Driscoll, Phys. Plasmas **26**, 122108 (2019).
[14]J. R. Danielson, F. Anderegg, and C. F. Driscoll, Phys. Rev. Lett. **92**, 245003 (2004).

[15]The current into the amplifier is $I(t)=-\epsilon_0\frac{d}{dt}\int_{sector}rd\theta dzE_r\propto\frac{d}{dt}\left(\frac{\partial\phi_m}{\partial r}\right)_{wall}\propto\frac{d}{dt}(\phi_m^{max})$, where ϕ_m is the mode potential. Therefore, $\int dtI(t)\propto\phi_m^{max}$.
[16]The term "localized waveform" is meant to be purely descriptive. It is not meant to imply that the observed entity has any characteristics beyond the localization the data show. Others have observed similar waveforms in directly driven experiments and given them varying interpretations. See, for example, Refs. 12 and 13.
[17]An alternative interpretation is that, for shorter traps, the $n=1$ mode frequency is high enough that the instability condition $\omega<l\omega_R$ is no longer satisfied (see Ref. 1). However, our ability to induce the instability at this frequency argues against this as the sole explanation.
[18]In contrast, trapping oscillations for modes of this amplitude tend to be much faster (with periods of tens of microseconds) and have less amplitude variation. See, for example, Ref. 14.